



1 **Brown carbon aerosol in rural Germany: sources, chemistry, and**
2 **diurnal variations**

3 *Feng Jiang^{1,2*}, Harald Saathoff^d, Junwei Song¹, Hengheng Zhang¹, Linyu Gao¹, and Thomas*
4 *Leisner^{1,3}*

5 ¹Institute of Meteorology and Climate Research, Karlsruhe Institute of Technology, 76344 Eggenstein–Leopoldshafen,
6 Germany

7 ²Institute of Applied Geosciences, Working Group for Environmental Mineralogy and Environmental System
8 Analysis, Karlsruhe Institute of Technology, 76131 Karlsruhe, Germany

9 ³Institute of Environmental Physics, Heidelberg University, 69120 Heidelberg, Germany

10 *Correspondence to:* Feng Jiang (feng.jiang@kit.edu) and Harald Saathoff (harald.saathoff@kit.edu)

11

12 **Abstract.** Brown carbon aerosol (BrC) is one major contributor to atmospheric air pollution in Europe, especially in
13 winter. Therefore, we studied the chemical composition, diurnal variation, and sources of BrC from 17th February to
14 16th March at a rural location in southwest Germany. In total, 178 potential BrC molecules (including 7 nitro aromatic
15 compounds, NACs) were identified in the particle phase comprising on average 63 ± 32 ng m⁻³, and 31 potential BrC
16 (including 4 NACs) molecules were identified in the gas phase contributing on average 6.2 ± 5.0 ng m⁻³ during the
17 whole campaign. The 178 potential BrC molecules only accounted for $2.3 \pm 1.5\%$ of the total organic mass, but can
18 explain $11 \pm 11\%$ of the total BrC absorption at 370 nm, assuming an average mass absorption coefficient at 370 nm
19 (MAC_{370}) of 9.5 m² g⁻¹. A few BrC molecules dominated the total BrC absorption. In addition, diurnal variations show
20 that gas phase BrC was higher at daytime and lower at night. It was mainly controlled by secondary formation (e.g.
21 photooxidation) and particle-to-gas partitioning. Correspondingly, the particle phase BrC was lower at daytime and
22 higher at nighttime. Secondary formation dominates the particle-phase BrC with $61 \pm 21\%$, while $39 \pm 21\%$ originated
23 from biomass burning. Furthermore, the particle-phase BrC showed decreasing light absorption due to photochemical
24 aging. This study extends the current understanding of real-time behaviors of brown carbon aerosol in the gas and
25 particle phase at a location characteristic for the central Europe.



26 **1. Introduction**

27 The Brown Carbon (BrC) aerosol has significant impact on air quality and climate, since it absorbs the solar radiation
28 in the near-ultraviolet and visible region (Laskin et al., 2015; Moise et al., 2015). Global simulation showed that the
29 mean radiative forcing of BrC aerosol was -0.43 W m^{-2} and 0.05 W m^{-2} at the surface and at the top of the atmosphere,
30 accounting for 15% of total radiative forcing by the absorbing aerosol (Park et al., 2010). In addition, global
31 measurements of BrC found that the average direct radiative effect of BrC absorption accounted between 7% to 48%
32 at the top of the atmosphere (Zeng et al., 2020).

33 Some typical molecules of BrC have been identified, such as nitro-aromatic compounds (NACs), imidazoles, and
34 polycyclic aromatic hydrocarbons (PAH), etc., (Jiang et al., 2022; Wu et al., 2018; Huang et al., 2018; Liu et al., 2023).

35 In western Europe, the concentration levels of NACs range between $1\text{--}20 \text{ ng m}^{-3}$, accounting for 0.3%–4% of total
36 absorption of BrC at UV wavelengths (Jiang et al., 2022; Mohr et al., 2013; Teich et al., 2017). In addition, imidazoles
37 were detected with concentrations ranging between $0.2\text{--}14 \text{ ng m}^{-3}$ in ambient aerosol samples from different
38 environments in Europe and China (Teich et al., 2016). Furthermore, parent-PAHs and carbonyl-OPAHs accounted
39 for on average $\sim 1.7\%$ of the overall absorption of methanol-soluble BrC in Urban Xi'an, Northwest China (Huang et
40 al., 2018). Even though many studies have investigated the chemical composition of brown carbon and calculated the
41 absorption contribution from BrC molecules, there are still many unknown brown carbon molecules to allow a
42 quantitative assessment of their sources and atmospheric impact.

43 Sources of BrC can be separated as primary emissions and secondary formation. The primary sources of BrC are
44 biomass burning and fossil fuel combustion (Andreae and Gelencser, 2006). On a global scale, a majority of BrC
45 aerosol mass is associated with biomass burning dominating BrC absorption (Zeng et al., 2020). The major secondary
46 sources of brown carbon are from oxidation of aromatic volatile organic compounds, such as toluene (Lin et al., 2015),
47 naphthalene (Siemens et al., 2022), ethylbenzene (Yang et al., 2022), and indole (Montoya-Aguilera et al., 2017; Jiang
48 et al., 2023), especially in the presence of NO_2 .

49 BrC in the atmosphere can be suspended in the gas phase or particle phase. However, only a few studies have
50 investigated the sources and chemical composition of BrC in the gas phase. For example, NACs in the gas phase were
51 highest during the daytime at a rural site in China (Salvador et al., 2021). The major sources of NACs were from
52 secondary formation on days without extensive biomass burning emissions, but mainly from primary emissions in
53 biomass burning events (Salvador et al., 2021). The source of nitrophenol, a typical BrC molecule, was mainly from
54 secondary formation overweighting losses by photolysis in polluted urban environments, Beijing (Cheng et al., 2021).



55 The major chromophores of BrC in the gas phase were rich in phenol- and protein-like substances in Xi'an, China,
56 during the summer (Chen et al., 2021). Therefore, the previous studies mainly focus on sources and chromophores of
57 BrC, especially NACs. However, the real-time diurnal variation and sources of BrC in the gas phase in the atmosphere
58 have rarely been investigated in central Europe.

59 Previous field studies have investigated the sources of BrC in the particle phase which are mainly from secondary
60 formation and primary emissions (Wang et al., 2019a; Moschos et al., 2018; Satish et al., 2017). In the central Europe,
61 the secondary biogenic organic aerosol (OA) contributes less BrC in summer. However, the primary and secondary
62 wood burning emissions dominated the BrC (Moschos et al., 2018). The primary emissions of BrC contributed more
63 to organic aerosol light absorption than those from secondary processes in the North China Plain, China (Wang et al.,
64 2019a). However, secondary sources for BrC were more important for absorption than primary ones in the Southeastern
65 Margin of Tibetan Plateau (Wang et al., 2019b). Loss pathways of BrC in the particle phase mainly comprise
66 photooxidation and photobleaching, but also dilution of BrC e.g. by rising boundary layer height influences its
67 concentration levels (Satish et al., 2017; Laskin et al., 2015; Moise et al., 2015). The absorption of BrC was high in
68 the early morning and later decreased due to the bleaching of chromophores (Wang et al., 2019a; Satish et al., 2017).
69 A diurnal cycle showed that secondary chromophores can be formed from photochemical oxidation after sunrise
70 followed by photobleaching of the chromophores under the oxidizing conditions as the day progressed (Wang et al.,
71 2019b). Lower BrC concentrations during noon were explained by the fact that planetary boundary layer heights were
72 highest during the middle of the day (Liu et al., 2023). However, also nighttime aqueous-phase chemistry can promote
73 the formation of secondary light absorbing compounds and the production of strongly absorbing particles (Wang et al.,
74 2019a). In addition, higher emissions of biomass burning BrC were observed at nighttime. Actually, the BrC in the
75 particle phase undergoes complex photochemical processing during the whole day. The time dependent sources and
76 diurnal variations of BrC in aerosol particles are still reported rarely and not well understood.

77 To better understand the chemical characterization, diurnal variation, and sources of BrC in central Europe, we
78 performed online measurements of BrC during February-March 2021 at a rural location in southwest Germany. In the
79 following, we will describe the experimental methods used in this study. Subsequently, the mass concentrations of BrC
80 in gas and particle phase will be determined. Furthermore, the contribution of BrC to light absorption in the particle
81 phase will be estimated. Then, the diurnal variations and sources of BrC in the gas and particle phase will be analyzed.
82 Finally, the atmospheric implications of our findings will be discussed.



83 **2. Experimental methods**

84 **2.1. Measurement site**

85 We performed particle and trace gas measurements from February 17th–March 16th 2021 at KIT Campus Nord, a rather
86 rural area in Germany (49°05'43.1"N 8°25'45.6"E). The sampling site is located at the building number 322 of the
87 IMK-AAF on KIT Campus Nord, as shown in Figure S1. The campus is mostly surrounded by the Hardwald forest
88 dominated by pine trees. The sampling site is also near some villages e.g. 3–4 km east of the village “Eggenstein-
89 Leopoldshafen”, 6–7 km northeast of the village “Neureut”, 3–4 km west of the village “Friedrichstal”, 4–5 km
90 northwest of the village “Stutensee”, and 5–6 km southeast of the village “Linkenheim”. Therefore, influences by
91 biomass burning emissions from wood stove combustion in these residential areas during winter time can be expected
92 (Thieringer et al., 2022). Furthermore, the city of Karlsruhe with 3000000 inhabitants is 10 km south of the
93 measurement site. The city includes industrial areas with a coal-fired power plant “Rheinhafen” and a refinery “MIRO”.
94 Therefore, the measurement site is potentially affected by different aerosol sources.

95 **2.2. Meteorological, aerosol particle, and traces gas instruments**

96 All instruments were set up in a temperature-controlled measurement building. The samples were collected above the
97 roof top about 8 m above ground level via stainless steel tubes and a PM_{2.5} and a TSP inlet as well as FEP tubes for the
98 VOC measurements. An overview of the instruments used and the parameters measured is given in Table S1 of the
99 Supplement.
100 Temperature, relative humidity (RH), pressure, wind speed, wind direction, precipitation, and global radiation were
101 measured by a meteorological sensor (WS700, Lufft GmbH; see Table S1) about 8 m above the ground level. The main
102 wind directions during the campaign were southwest, northeast, and southeast, since winds were channeled by the
103 Rhine River valley. O₃ and NO₂ were measured with standard gas monitors (Table S1). The particle number
104 concentrations (>2.5 nm) were measured by a water-based condensation particle counter (CPC3789, TSI Inc.). PM_{2.5}
105 was measured by an optical particle counter (OPC-FIDAS 200, Palas Inc.). The particle number size distributions were
106 measured by a nanoparticle sizer (NanoScan, TSI Inc.) ranging from 10–410 nm at a time resolution of 1 min. Black
107 carbon (BC) concentrations were measured with aethalometers (AE33, Aerosol Magee Scientific).



108 **2.3. Online FIGAERO-CIMS measurement and identifications of potential BrC molecules**

109 The individual organic compounds in both the gas and particle phase were measured with a filter inlet for gases and
110 aerosols coupled to a high-resolution time-of-flight chemical ionization mass spectrometer (FIGAERO-HR-ToF-CIMS,
111 Aerodyne Research Inc. hereafter CIMS) employing iodide (I^-) for chemical ionization (Lopez-Hilfiker et al., 2014;
112 Jiang et al., 2022). During the gas-phase measurement, the ambient air was sampled via a fluorinated ethylene
113 propylene (FEP) tube of 4.5 m length (flow rate 8 L min^{-1} , residence time 0.9 s). At the same time, the particles were
114 collected on a Teflon (Polytetrafluoroethylene, PTFE) filter via a separate sampling port connected to a $PM_{2.5}$ inlet
115 (total flow rate 16.7 L min^{-1}) and an 8 m long stainless-steel tube. The loading time and sampling flow of Teflon filters
116 were 30 minutes and 4 L min^{-1} , respectively. At regular intervals (46 min), the gas-phase measurement was switched
117 off and particles on the filter were desorbed by a flow of ultra-high-purity nitrogen (99.9999 %) heated from room
118 temperature to $200 \text{ }^\circ\text{C}$ over the course of 35 min (Lopez-Hilfiker et al., 2014; Huang et al., 2019a). The resulting mass
119 spectral signal evolutions as a function of desorption temperature are termed thermograms (Lopez-Hilfiker et al., 2014).
120 Integration of thermograms of individual compounds yielded their signal in counts per second, which were converted
121 to mass concentrations using an average sensitivity of $22 \text{ count s}^{-1} \text{ ppt}^{-1}$ (Lopez-Hilfiker et al., 2014). Please note that
122 the sensitivity of CIMS for different organic compounds varies by a few orders of magnitude. Sensitivity uncertainties
123 were taken into account in the calculation of the overall uncertainties of CIMS concentrations ($\pm 60\%$) following the
124 approach by Thompson et al. (2017).

125 During the measurements, the mass resolution of FIGAERO-CIMS was relatively stable with about $4000 \text{ m}/\Delta$. The
126 interference from isomers with different vapor pressures or thermal fragmentation of larger oligomeric molecules can
127 lead to more complex, multimodal and broader thermograms (Lopez-Hilfiker et al., 2014). The signal integration can
128 include the different isomers or thermal fragmentation of larger oligomers. Therefore, the isomers or thermal
129 decomposition can lead to increase errors of estimating the organic mass concentrations. In this study, atmospheric
130 mass concentrations of BrC were detected by FIGAERO-CIMS. These values have high uncertainty with several orders
131 of magnitude. However, this is still a reasonable method to measure the organic aerosol in atmosphere. The raw data
132 were analysed by using the toolkit Tofware (v3.1.2, Tofwerk, Thun, Switzerland, and Aerodyne, Billerica) with the
133 Igor Pro software (v7.08, Wavemetrics, Portland, OR). Gas phase background was determined by sampling zero air
134 (high purity synthetic air). Particle phase backgrounds were assessed by putting an additional Teflon filter upstream of
135 the particle phase sampling port during the deposition (Huang et al., 2019a; Lee et al., 2018).



136 We observed typically about 1500 mass peaks from particles and 120 mass peaks in gases corresponding to different
137 oxygenated organic compounds by using FIGAERO-CIMS. Individual compounds were assigned to the mass peaks
138 by fitting, $C_cH_hO_oN_n$, different numbers of atoms: c carbon, h hydrogen, o oxygen, n nitrogen (Lopez-Hilfiker et al.,
139 2014). A double bond equivalent (DBE) can be calculated as follows (Daumit et al., 2013):

$$140 \quad DBE = \frac{n-h}{2} + c + 1 \quad (1)$$

141 Lin et al. (2018) assigned potential brown carbon compounds in the plot of DBE vs the number of carbon atoms per
142 molecule. They employed high-resolution mass spectrometry to analyze biomass burning organic aerosol. We used
143 this method to find potential BrC molecules (Jiang et al., 2022). The potential BrC molecules in the particle and gas
144 phase were shown in Table S2 and S3.

145 **2.4. Particle light absorption from aethalometer measurements**

146 In the aethalometer AE33 (Magee Scientific), aerosol particles are continually sampled on a quartz filter and the optical
147 attenuation is measured with time resolutions 1 minute at seven wavelengths (370, 470, 520, 590, 660, 880, and 950
148 nm) during this campaign. The light absorption at seven wavelengths was calculated from the measured attenuation.
149 Attenuation is measured on two spots with different sample flows and on the reference spot without sample flow. The
150 two loading spots with different flow are used to allow for loading effect corrections (Drinovec et al., 2015). The light
151 absorption of aerosol particles on the filter is also influenced by scattering of light within filter which will enhance the
152 light absorption. In this measurement, we used the default value (1.57) to do the scattering correction (Drinovec et al.,
153 2015). The BC mass concentration is calculated from the change in optical attenuation at 880 nm in the selected time
154 interval using the mass absorption cross section $7.77 \text{ m}^2 \text{ g}^{-1}$ (Gundel et al., 1984), since other aerosol particles (organic
155 aerosol or mineral) have less absorption at this wavelength and major absorption is contributed from BC alone. The
156 attenuation mass absorption coefficients of AE33 from 370 – 880nm were 18.47, 14.54, 13.14, 11.58, 10.35, and 7.77
157 $\text{m}^2 \text{ g}^{-1}$, respectively.

158 We assumed negligible absorption by dust and thus, Abs_λ can be divided into BC and BrC absorption. Therefore, the
159 $Abs_{BrC}(\lambda)$ can be calculated as follows:

$$160 \quad Abs_{BrC}(\lambda) = Abs(\lambda) - Abs(880) \times \left(\frac{\lambda}{880}\right)^{-AAE_{BC}} \quad (2)$$

161 Where $Abs_{BrC}(\lambda)$ is the absorption caused by BrC at $\lambda = 370, 470, 520, 590, \text{ or } 660 \text{ nm}$, the $Abs(\lambda)$ is total absorption
162 by AE33, the $Abs(880)$ is the light absorption at 880 nm, and the AAE_{BC} is 1.



163 The fraction of wood burning black carbon (BC_{wb}) was calculated by using the Aethalometer model (Sandradewi et
164 al., 2008a; Sandradewi et al., 2008b):

$$165 \quad BC_{wb} = \left[\frac{b_{abs}(470nm) - b_{abs}(950nm) * \left(\frac{470}{950}\right)^{-aff}}{\left(\frac{470}{950}\right)^{-awb} - \left(\frac{470}{950}\right)^{-aff}} \right] / b_{abs}(950nm) * BC \quad (3)$$

166 Where two pairs of Ångström exponents values were utilized to obtain BC associated with fossil fuel (BC_{ff}) and wood
167 burning (BC_{wb}): aff and awb of 0.95 and 1.60 were applied (Saarikoski et al., 2021).

168 3. RESULTS AND DISCUSSION

169 3.1. Overview of the field observations

170 Figures S1 and S2 give an overview of the measurement location and the meteorological parameters, traces gases,
171 particle concentrations, and their optical properties during the campaign. The major wind directions at KIT Campus
172 Nord, 3 km east of the village of Eggenstein-Leopoldshafen, were northeast and southwest (Figure S1) caused by
173 channeling of the wind in the Rhine valley. The average wind speeds were 1.1 ± 0.8 (average \pm standard deviation) m
174 s⁻¹. Depending on meteorological conditions, local sources and regional transport had a major impact on air quality in
175 Leopoldshafen in summer (Shen et al., 2019). As shown in Figure S1 and S5, O₃ had diurnal variations with peaks at
176 daytime and an average of $41.3 \pm 26.2 \mu\text{g m}^{-3}$ during the campaign. In contrast, the relative humidity (RH) showed
177 diurnal variations with peaks at nighttime and an average of $68 \pm 16\%$ during the campaign (Figure S5). The average
178 temperature during the winter campaign was $6.5 \pm 5.6 \text{ }^\circ\text{C}$ and slowly increased from beginning to the end of the
179 campaign. NO₂ had high concentrations at some periods e.g. from 20th to 23th February with $22 \pm 8.6 \mu\text{g m}^{-3}$ and from
180 2nd to 4th March with $35 \pm 14 \mu\text{g m}^{-3}$. The average SO₂ concentration was $0.8 \pm 1.0 \mu\text{g m}^{-3}$, significantly lower than the
181 NO₂ concentrations. During some Saharan dust events, the PM_{2.5} and PM₁₀ mass concentrations were 21 ± 6 and $45 \pm$
182 $20 \mu\text{g m}^{-3}$, respectively, from 18th to 26th February and 19 ± 6 and $24 \pm 7 \mu\text{g m}^{-3}$, respectively, from 1st to 4th March as
183 indicated by red boxes in the lowest panel of Figure S1. In addition, BC showed many spikes and a good correlation
184 ($r^2 = 0.8$) with NO₂ (Figure S2). This indicates that there were many combustion events during the campaign (Figure
185 S3). The absorption Ångström exponents of particles between 370 and 520 nm (AAE₃₇₀₋₅₂₀) and AAE₆₆₀₋₉₅₀ had diurnal
186 variations with peaks at nighttime. We calculated the fraction of wood burning BC and fossil fuel BC as shown in
187 Figure S2 using the Aethalometer model (Sandradewi et al., 2008a). During the winter campaign, the biomass burning
188 BC was on average $0.73 \pm 0.6 \mu\text{g m}^{-3}$, mostly higher than $0.3 \pm 0.3 \mu\text{g m}^{-3}$ for fossil fuel BC. The AAE₃₇₀₋₅₂₀, AAE₆₆₀₋



189 $_{950}$, biomass burning BC, and NO_2 values were enhanced from 20th to 23th February and 2nd to 4th March. This indicates
190 that strong biomass burning (BB) events were on these days. During this winter campaign, the BrC absorption
191 accounted for ~40% of total absorption caused by BC and BrC. This points to the at least regional or seasonal
192 importance of BrC absorption which has an important effect on air quality and climate.

193 3.2. Mass concentrations and volatility of brown carbon molecules

194 Figure 1 shows an overview of levoglucosan concentrations, BC concentrations, absorption of brown carbon at 370
195 nm ($b_{\text{brc}370}$), $\text{AAE}_{370-520}$, volatility and mass concentrations of 178 brown carbon molecules identified in the particle
196 phase and 31 brown carbon molecules in the gas phase during the whole winter campaign. We identified 178 BrC
197 molecules showing a good correlation ($R=0.8$) with the absorption at 370 nm (abs_{370}) of BrC (Figure S6). This indicates
198 that it is meaningful to extract these 178 BrC molecules from more than one thousand and five hundred molecules
199 detected by FIGAERO-CIMS based on the double bond equivalent/carbon number ratio (DBE/C) of each molecule
200 being higher than 0.5 and less than 0.9. The levoglucosan had a good correlation ($r=0.7$) with BC. This also indicates
201 that BC was mainly emitted from biomass burning during the winter campaign. Consistently, biomass burning BC
202 accounted for 70% of total BC as we discussed above. The 178 BrC molecules detected in the particle phase correspond
203 to an average mass concentrations of $63 \pm 32 \text{ ng m}^{-3}$. In addition, the nitro aromatic compounds (NACs) were also
204 detected during the winter campaign. The mass concentration of $\sum \text{NACs}$ in the gas phase and particle phase were 1.2
205 $\pm 0.9 \text{ ng m}^{-3}$ and $10.7 \pm 10.7 \text{ ng m}^{-3}$, respectively (Table S4 and S5). Mohr et al. (2013) found that five BrC molecules
206 (nitro aromatic compounds) were 20 ng m^{-3} detected by CIMS during winter in Detling, United Kingdom. Jiang et al.
207 (2022) measured an average concentration of five BrC molecules (nitro aromatic compounds) of $1.6 \pm 0.9 \text{ ng m}^{-3}$ during
208 the winter at a kerbside in downtown Karlsruhe, a city in southwest Germany and close to our measurement site.
209 Therefore, the detection of the 178 BrC molecules allows more complete assessment of the BrC concentrations during
210 this winter campaign. Their concentrations were significantly higher for biomass burning (BB) events e.g. $103 \pm 31 \text{ ng}$
211 m^{-3} at BB event 1 and $102 \pm 34 \text{ ng m}^{-3}$ at BB event 2, respectively. In addition, the absorption of brown carbon at 370
212 nm ($b_{\text{brc}370}$) had high peaks with $\sim 100 \text{ Mm}^{-1}$ and the $\text{AAE}_{370-520}$ of particles increased from ~ 1.5 to ~ 2 during the BB
213 events. The average concentration of BrC in the gas phase was $6.2 \pm 5.0 \text{ ng m}^{-3}$ during the winter campaign. At BB
214 events, their concentration can reach up to 26 ng m^{-3} . Therefore, biomass burning had a significant impact on optical
215 properties of aerosol and brown carbon concentrations. The lowermost panel of Figure 1 shows the temporal variation
216 of the average volatility of brown carbon molecules in the gas and particle phase. The average volatility or saturation



217 concentration ($\log_{10}C_{\text{sat}}$) of BrC in the particle phase was with $-1.1 \pm 0.5 \mu\text{g m}^{-3}$ lower than $0.9 \pm 0.6 \mu\text{g m}^{-3}$ of BrC in
218 the gas phase during the winter campaign. Organic compounds with $\log_{10}C_{\text{sat}}$ lower than $-4.5 \mu\text{g m}^{-3}$, between -4.5
219 and $-0.5 \mu\text{g m}^{-3}$, between -0.5 and $2.5 \mu\text{g m}^{-3}$, and between 2.5 and $6.5 \mu\text{g m}^{-3}$ are termed extremely low-volatility
220 organic compounds (ELVOCs), low-volatility organic compounds (LVOCs), semi-volatile organic compounds
221 (SVOCs), and intermediate-volatility organic compounds (IVOCs), respectively (Donahue et al., 2009). Therefore,
222 BrC in the particle phase can be classified on average to the LVOCs and BrC in the gas phase to the SVOCs.

223 3.3 Absorption contribution of nitroaromatic compounds and potential brown carbon molecules

224 Black carbon dominated light absorption of aerosol particles with a contribution of 100% at 880 nm and decreasing to
225 73% at 370 nm. With shorter wavelengths, the brown carbon absorption contribution significantly increased
226 contributing 27% of total aerosol absorption at 370 nm (Figure 2a). Since the online instrument to measure total organic
227 aerosol mass, the AMS, wasn't available during this campaign, we estimated the total organic mass as a fraction of 40%
228 of $\text{PM}_{2.5}$ which is a typical fraction for this season and region (Song et al., 2022; Huang et al., 2019b). Based on this
229 assumption, the average organic aerosol mass concentration calculates to $4.2 \pm 3.0 \mu\text{g m}^{-3}$. We calculated the light
230 absorption of NACs by using molecular MAC_{365} (Xie et al., 2017). Based on this, the mean light absorption of the sum
231 of the seven NACs was calculated to be $0.1 \pm 0.1 \text{ Mm}^{-1}$, contributing to $1.3 \pm 1.4\%$ of total BrC absorption at 370 nm,
232 but they only contributed $0.34 \pm 0.32\%$ of the total organic mass.

233 In order to calculate the light absorption from the other 171 potential brown carbon molecules identified, we assumed
234 an average MAC value of $9.5 \text{ m}^2 \text{ g}^{-1}$ at 370 nm for all BrC molecules to estimate their absorption (Jiang et al., 2022).
235 So far, the MAC_{370} of most potential brown carbon molecules are still unknown. In addition, since the BrC molecules
236 detected by FIGAERO-CIMS could have isomers effect, we did not calibrate mass absorption coefficients of 171
237 potential BrC. Therefore, it could have uncertainty to estimate the absorption of total BrC absorption based on this
238 assumption. However, it is still a reasonable method to estimate the BrC absorption. Based on this assumption, we
239 calculated the light absorption of the 171 brown carbon molecules identified to $0.5 \pm 0.3 \text{ Mm}^{-1}$ at 370 nm as average
240 for the whole winter campaign. This is half the values Jiang et al. (2022) found as mean light absorption of 316 potential
241 BrC molecules of $1.2 \pm 0.2 \text{ Mm}^{-1}$ at 365 nm for downtown Karlsruhe in winter. Relative to this total organic aerosol
242 particle mass and the measured brown carbon absorption, the 171 identified brown carbon molecules and 7 NACs only
243 accounted for $2.3 \pm 1.5\%$ of the total organic mass, but explain $11 \pm 11\%$ of total brown carbon absorption at 370 nm
244 (Figure 2b and 2c). Palm et al. (2020) found that particulate nitroaromatic compounds (BrC molecules) can explain 29



245 $\pm 15\%$ of average BrC light absorption at 405 nm, despite accounting for just $4 \pm 2\%$ of average OA mass in fresh
246 wildfire plumes. Mohr et al. (2013) found that five nitroaromatic compounds (BrC molecules) are potentially important
247 contributors to absorption at 370 nm measured by an aethalometer and account for $4 \pm 2\%$ of UV light absorption by
248 brown carbon in Detling, United Kingdom during winter. Jiang et al. (2022) determined a mean light absorption of the
249 316 potential BrC molecules accounting for $32 \pm 15\%$ of methanol-soluble BrC absorption at 365nm, but only
250 accounted for $2.5 \pm 0.6\%$ of the organic aerosol mass. Therefore, even small mass fractions of strongly absorbing
251 brown carbon molecules can dominate the brown carbon absorption.

252 **3.4 Diurnal variations and sources of BrC in the gas phase**

253 As shown in Figure 3a, the 31 gas-phase BrC (GBrC) molecules showed higher concentrations at daytime (09:00-
254 17:00) and lower concentration between evening and early morning (18:00-08:00). Salvador et al. (2021) also found
255 that 16 gas-phase nitro-aromatic compounds (BrC molecules) measured by FIGAERO-CIMS were higher during
256 daytime and lower at nighttime during winter in rural China. As discussed above, strong biomass burning emission
257 were mostly observed at evening and early morning hours. However, gas-phase BrC had no peaks during those time
258 periods. Therefore, the primary emission from biomass burning was not a major source for GBrC at KIT Campus Nord.
259 It seems to be mainly controlled by secondary formation (e.g. photochemical smog) or/and particle-to-gas partitioning
260 (Salvador et al., 2021).

261 To demonstrate how secondary formation and partitioning control the gas-phase BrC in rural Germany, we plotted
262 diurnal profiles of the average volatility and volatility fractions of IVOC, SVOC, and LVOC of the gas-phase BrC
263 (Figure 3b). The LVOC of BrC increased at evenings and decreased at daytime. In contrast, the IVOC of BrC increased
264 at daytime and reached $\sim 17\%$ of total $\log_{10}C^*$ (volatility) in gas-phase BrC while SVOC remained with a relative
265 constant fraction ($\sim 60\%$). Furthermore, the IVOC fraction of BrC in the particle-phase was only 1.5% with a flat
266 diurnal profile (Figure S7). The O/C ratio of gas-phase BrC also increased during daytime (Figure 3d). Therefore, the
267 higher fraction of IVOC in the gas phase at daytime could be mainly caused by secondary formation e.g. photochemical
268 aging because of higher concentrations of O_3 at same time (Figure 3c) (Salvador et al., 2021). Figure S8 shows that
269 BrC in the gas phase had a good correlation ($r=0.4$) with temperature. This explains why the temperature shows a
270 similar diurnal profile as the gas-phase BrC. Therefore, particle-to-gas partitioning was also an important source for
271 gas-phase BrC. However, our results are not consistent with previous studies where 16 BrC molecules in gas phase
272 were mainly from primary emission during the biomass burning evenings and secondary formation during the clear



273 days in rural China (Salvador et al., 2021). Our measurement site was several km away from biomass burning sites
274 with ~7-10 km. And the 31 BrC in the gas-phase sum up to $6.2 \pm 5.0 \text{ ng m}^{-3}$, significantly lower than 1720 ng m^{-3} of
275 16 BrC (Salvador et al., 2021). Cheng et al. (2021) found that secondary formation was a strong source for five BrC
276 molecules in the gas-phase. Therefore, BrC in the gas-phase are less influenced from primary emissions from biomass
277 burning but are mainly controlled by secondary formation and partitioning in rural Germany.

278 3.5 Diurnal variations and sources of BrC in the particle phase

279 The 178 BrC molecules in the particle phase (PBrC) exhibited two peaks in the diurnal profile (Figure 3a) averaged
280 over the whole winter campaign. They increased from 19:00 to 01:00 with a peak at $82 \pm 35 \text{ ng m}^{-3}$ around midnight.
281 Then the PBrC slowly decreased after midnight. However, they increased again from 6:00 to 08:00 and forming a
282 second peak with $76 \pm 50 \text{ ng m}^{-3}$ in the morning. During daytime, they decreased reaching lowest values with 47 ± 24
283 ng m^{-3} at 14:00-15:00. During the nighttime and morning hours, the higher mass concentrations of PBrC were caused
284 by residential wood burning emissions. Consistently, higher $\text{PM}_{2.5}$ concentration levels at nighttime at a rural site near
285 Karlsruhe, Germany, could be assigned to wood burning emissions from wood stove operation during winter
286 (Thieringer et al., 2022). The low mass concentrations of PBrC at daytime could be explained by photobleaching and
287 evaporation of BrC, and/or dilution by the increasing planetary boundary layer heights (Satish et al., 2017). Satish et
288 al. (2017) found that BrC over the Indo-Gangetic Plain had two peaks of BrC at evening and morning hours, and lowest
289 values during daytime.

290 To determine the sources of brown carbon, we used the edge approach (Day et al., 2015). It allows to estimate the
291 contribution of primary biomass burning (BB) to the measured BrC concentrations using levoglucosan as a primary
292 source tracer. This approach is analogous to the widely used elemental carbon (EC) tracer approach, in which EC is
293 used to distinguish the primary organic carbon (POC) and secondary organic carbon (SOC) in total organic carbon
294 (OC) measurements (Day et al., 2015; Cabada et al., 2004). Levoglucosan (lev) and BrC were measured online by the
295 same instruments and under the same conditions. As discussed above, we observed a good correlation ($r=0.8$) between
296 levoglucosan and BC during the winter campaign. Therefore, levoglucosan is a suitable tracer for primary BB. Please
297 note that we did not calibrate the sensitivities of levoglucosan detected by FIGAERO-CIMS. Therefore, it could cause
298 some uncertainties to estimate brown carbon from biomass burning and secondary formation. Figure 4a shows that the
299 blue points can be used as edge points to determine the ratio of BrC/levoglucosan at the primary emissions from



300 biomass burning. The relative contributions of primary emissions (BB) and secondary (sec) formation for total BrC
301 molecules were estimated using the following expression:

$$302 \quad BrC_{BB} = \left(\frac{[BrC]}{[lev]_{BB}} \right) * [lev.]$$

$$303 \quad [BrC_{sec}] = [BrC_{Tot}] - [BrC_{BB}]$$

304 Where $([BrC]/[lev])_{BB}$ is the ratio of the concentration of the BrC to that of levoglucosan in the primary emissions from
305 biomass burning and this value is 1.9 ± 0.1 (Figure 4a), BrC_{BB} and BrC_{sec} are the fractions of BrC generated through
306 biomass burning and secondary production, respectively, BrC_{Tot} and $lev.$ are the measured concentrations of BrC and
307 levoglucosan during the winter campaign. Using this approach, we calculated the diurnal profiles of BrC from primary
308 emissions (BrC_{BB}) and secondary formation (BrC_{sec}) shown in Figure 4b. The mass fraction of BrC_{sec} increased at
309 daytime and decreased at evening. This indicates that the secondary formation for BrC in the particle phase was
310 enhanced during daytime, facilitated by the higher levels of oxidants e.g. O_3 (Figure 3c). The mass fraction of BrC_{BB}
311 had two peaks at early morning and in the evening hours, respectively. This may be caused by residential wood burning
312 emissions. BrC_{BB} accounts for $39 \pm 21\%$ of the total BrC as averaged for the whole measurement period. During
313 biomass burning events, the BrC_{BB} is a major mass fraction for total BrC that accounts for $61 \pm 13\%$ during BB-event1
314 and $65 \pm 12\%$ during BB-event-2, respectively. Therefore, the primary emissions of BrC have a significant impact on
315 BrC, especially, at biomass burning events. However, on average over the whole campaign, BrC_{sec} dominates the
316 mass fraction of BrC with $61 \pm 21\%$. Therefore, the secondary formation can be considered as an important source for
317 BrC in rural Germany. Consistently, secondary formation from biomass burning emission is important for the brown
318 carbon absorption in the Switzerland, the central Europe. (Moschos et al., 2018). Secondary sources for BrC were more
319 important for absorption than primary ones in the Southeastern Margin of the Tibetan Plateau (Wang et al., 2019b).

320 To further investigate the oxidation of BrC in the particle phase we plotted, the diurnal profiles of O/C ratios of BrC
321 during the whole campaign was measured, as shown in Figure 5. The O/C ratio of BrC increased at daytime and
322 decreased at nighttime. The ozone had the same diurnal profile as the O/C ratio of BrC. In addition, the O/C ratio of
323 BrC had a positive correlation ($r=0.8$) with ozone. This indicates that the BrC was photo-oxidized leading to an increase
324 of the O/C ratio of BrC. In contrast, the light absorption of BrC at 370 nm (b_{brc370}) and the double bond equivalent
325 (DBE) decreased at daytime and increased at nighttime. During daytime, the absorption of brown carbon at 370 nm
326 decreased due to lower DBE and higher O/C values of brown carbon caused by photooxidation. This is in accordance



327 with previous studies where atmospheric photooxidation diminishes light absorption of primary brown carbon aerosol
328 from biomass burning (Sumlin et al., 2017). Oxidative whitening can reduce light absorption of brown carbon during
329 the day (Hems et al., 2021).

330 **Conclusions**

331 The chemical composition, diurnal variation, and sources of brown carbon aerosol were investigated during February-
332 March 2021 in a rural area, at KIT Campus Nord, a location characteristic for central Europe. The 178 brown carbon
333 molecules (including 7 nitro aromatic compounds, NACs) identified in the particle phase contributed on average $63 \pm$
334 32 ng m^{-3} and 31 brown carbon molecules (including 4 NACs) identified in the gas phase contributed on average 6.2
335 $\pm 5.0 \text{ ng m}^{-3}$ during the whole campaign. During dedicated biomass burning events, BrC concentrations in the particle
336 phase were significantly higher with up to $\sim 100 \text{ ng m}^{-3}$. The 178 identified brown carbon molecules only accounted
337 for $2.3 \pm 1.5\%$ of the total organic mass, but explained $11 \pm 11\%$ of the total brown carbon absorption at 370 nm,
338 assuming a MAC_{370} as $9.5 \text{ m}^2 \text{ g}^{-1}$. This shows that a small fraction of the brown carbon molecules dominates the overall
339 absorption. This indicates the great importance of identifying these molecules, the strong absorbers, to predict aerosol
340 absorption.

341 Diurnal variations show that the particle-phase BrC had two peaks at early morning and evening hours, respectively.
342 These were mainly caused by residential wood burning emissions. In contrast, the gas-phase BrC showed higher
343 concentrations at daytime and lower concentrations at nighttime. The gas-phase BrC molecules were mainly controlled
344 by secondary formation (e.g. by photochemical processes) and particle-to-gas partitioning. The two main sources
345 contributed to particle-phase BrC were primary emission from biomass burning and secondary formation. Secondary
346 formation, e.g. by photooxidation, is an important source of particle-phase BrC corresponding to increasing O/C ratios
347 of BrC during daytime and a positive correlation ($r=0.8$) with ozone concentrations. In addition, the DBE of the
348 particle-phase decreased during daytime. This indicates that the absorption of brown carbon at 370 nm decreased due
349 to lower DBE and higher O/C ratio due to the photooxidation of brown carbon. Compared with previous measurements
350 in central Europe (Lukács et al., 2007; Zhang et al., 2020), our study found that secondary formation, e.g.,
351 photochemical processes, was an important source for BrC in gas and particle phases. To improve air quality in winter,
352 we need to reduce biomass burning emissions (e.g., regulate wood stoves) but also reduce the precursors to form



353 secondary aerosol. Overall, this study provides good insight into the light absorption, sources, and diurnal variation
354 from real-time observations of brown carbon molecules in central Europe by using mass spectrometry and aethalometer.

355 ***Data availability***

356 Data are available upon request to the corresponding author.

357 **Competing interests**

358 At least one of the (co-)authors is a member of the editorial board of Atmospheric Chemistry and Physics

359 **Author contributions**

360 FJ and HS designed the measurement campaign. FJ, LG, JS, and HS performed the experimental work. FJ did
361 FIGAERO-CIMS and AE33 data analysis. HS and HZ processed the trace gas and meteorological data, respectively.
362 TL gave general comments for this paper. FJ wrote the paper with contributions from all co-authors.

363 **ACKNOWLEDGMENTS**

364 The authors gratefully thank the staff of IMK-AAF for providing substantial technical support during the field
365 campaigns under COVID conditions. Furthermore, Feng Jiang and Junwei Song are thankful for the support from the
366 China Scholarship Council (CSC).

367



368 REFERENCES

- 369 Andreae, M. O., and Gelencser, A.: Black carbon or brown carbon? The nature of light-absorbing carbonaceous
370 aerosols, *Atmos. Chem. Phys.* 6, 3131-3148, <https://doi.org/10.5194/acp-6-3131-2006>, 2006.
- 371 Cabada, J. C., Pandis, S. N., Subramanian, R., Robinson, A. L., Polidori, A., and Turpin, B.: Estimating the secondary
372 organic aerosol contribution to PM_{2.5} using the EC tracer method, *Aerosol Sci. Technol.* 38, 140-155,
373 <https://doi.org/10.1080/02786820390229084>, 2004.
- 374 Chen, Q. C., Chen, Q., Hua, X. Y., Guan, D. J., and Chang, T.: Gas-phase brown carbon: Absorbance and chromophore
375 types, *Atmos. Environ.* 264, <https://doi.org/10.1016/j.atmosenv.2021.118646>, 2021.
- 376 Cheng, X., Chen, Q., Li, Y., Huang, G., Liu, Y., Lu, S., Zheng, Y., Qiu, W., Lu, K., Qiu, X., Bianchi, F., Yan, C.,
377 Yuan, B., Shao, M., Wang, Z., Canagaratna, M. R., Zhu, T., Wu, Y., and Zeng, L.: Secondary Production of Gaseous
378 Nitrate Phenols in Polluted Urban Environments, *Environ. Sci. Technol.* 55, 4410-4419,
379 <https://doi.org/10.1021/acs.est.0c07988>, 2021.
- 380 Daumit, K. E., Kessler, S. H., and Kroll, J. H.: Average chemical properties and potential formation pathways of highly
381 oxidized organic aerosol, *Farad. Disc.* 165, 181-202, <https://doi.org/10.1039/c3fd00045a>, 2013.
- 382 Day, M. C., Zhang, M. H., and Pandis, S. N.: Evaluation of the ability of the EC tracer method to estimate secondary
383 organic carbon, *Atmos. Environ.* 112, 317-325, <https://doi.org/10.1016/j.atmosenv.2015.04.044>, 2015.
- 384 Donahue, N. M., Robinson, A. L., and Pandis, S. N.: Atmospheric organic particulate matter: From smoke to secondary
385 organic aerosol, *Atmos. Environ.* 43, 94-106, <https://doi.org/10.1016/j.atmosenv.2008.09.055>, 2009.
- 386 Drinovec, L., Mocnik, G., Zotter, P., Prevot, A. S. H., Ruckstuhl, C., Coz, E., Rupakheti, M., Sciare, J., Müller, T.,
387 Wiedensohler, A., and Hansen, A. D. A.: The "dual-spot" Aethalometer: an improved measurement of aerosol black
388 carbon with real-time loading compensation, *Atmos. Meas. Tech.* 8, 1965-1979, [https://doi.org/10.5194/amt-8-1965-](https://doi.org/10.5194/amt-8-1965-2015)
389 2015, 2015.
- 390 Gundel, L. A., Dod, R. L., Rosen, H., and Novakov, T.: The relationship between optical attenuation and black carbon
391 concentration for ambient and source particles, *Sci. Total Environ.* 36, 197-202, [https://doi.org/10.1016/0048-](https://doi.org/10.1016/0048-9697(84)90266-3)
392 9697(84)90266-3, 1984.
- 393 Hems, R. F., Schnitzler, E. G., Liu-Kang, C., Cappa, C. D., and Abbatt, J. P. D.: Aging of Atmospheric Brown Carbon
394 Aerosol, *ACS Earth Space Chem.* 5, 722-748, <https://doi.org/10.1021/acsearthspacechem.0c00346>, 2021.
- 395 Huang, R.-J., Yang, L., Cao, J., Chen, Y., Chen, Q., Li, Y., Duan, J., Zhu, C., Dai, W., Wang, K., Lin, C., Ni, H.,
396 Corbin, J. C., Wu, Y., Zhang, R., Tie, X., Hoffmann, T., O'Dowd, C., and Dusek, U.: Brown Carbon Aerosol in Urban
397 Xi'an, Northwest China: The Composition and Light Absorption Properties, *Environ. Sci. Technol.* 52, 6825-6833,
398 <https://doi.org/10.1021/acs.est.8b02386>, 2018.



- 399 Huang, W., Saathoff, H., Shen, X., Ramisetty, R., Leisner, T., and Mohr, C.: Chemical Characterization of Highly
400 Functionalized Organonitrates Contributing to Night-Time Organic Aerosol Mass Loadings and Particle Growth,
401 *Environ. Sci. Technol.* 53, 1165-1174, <https://doi.org/10.1021/acs.est.8b05826>, 2019a.
- 402 Huang, W., Saathoff, H., Shen, X. L., Ramisetty, R., Leisner, T., and Mohr, C.: Seasonal characteristics of organic
403 aerosol chemical composition and volatility in Stuttgart, Germany, *Atmos. Chem. Phys.* 19, 11687-11700,
404 <https://doi.org/10.5194/acp-19-11687-2019>, 2019b.
- 405 Jiang, F., Song, J. W., Bauer, J., Gao, L. Y., Vallon, M., Gebhardt, R., Leisner, T., Norra, S., and Saathoff, H.:
406 Chromophores and chemical composition of brown carbon characterized at an urban kerbside by excitation-emission
407 spectroscopy and mass spectrometry, *Atmos. Chem. Phys.* 22, 14971-14986, [https://doi.org/10.5194/acp-22-14971-](https://doi.org/10.5194/acp-22-14971-2022)
408 2022, 2022.
- 409 Jiang, F., Siemens, K., Linke, C., Li, Y., Gong, Y., Leisner, T., Laskin, A., and Saathoff, H.: Molecular analysis of
410 secondary organic aerosol and brown carbon from the oxidation of indole. *Atmos. Chem. Phys.* 24(4), 2639-2649.
411 <https://doi.org/10.5194/acp-24-2639-2024>, 2024
- 412 Laskin, A., Laskin, J., and Nizkorodov, S. A.: Chemistry of Atmospheric Brown Carbon, *Chem. Rev.* 115, 4335-4382,
413 <https://doi.org/10.1021/cr5006167>, 2015.
- 414 Lee, B., Lopez-Hilfiker, F. D., D'Ambro, E. L., Zhou, P. T., Boy, M., Petaja, T., Hao, L. Q., Virtanen, A., and Thornton,
415 J. A.: Semi-volatile and highly oxygenated gaseous and particulate organic compounds observed above a boreal forest
416 canopy, *Atmos. Chem. Phys.* 11547-11562, <https://doi.org/10.5194/acp-18-11547-2018>, 2018.
- 417 Lin, P., Liu, J., Shilling, J. E., Kathmann, S. M., Laskin, J., and Laskin, A.: Molecular characterization of brown carbon
418 (BrC) chromophores in secondary organic aerosol generated from photo-oxidation of toluene, *Phys. Chem. Chem.*
419 *Phys.* 17, 23312-23325, <https://doi.org/10.1039/c5cp02563j>, 2015.
- 420 Liu, X., Wang, H., Wang, F., Lv, S., Wu, C., Zhao, Y., Zhang, S., Liu, S., Xu, X., Lei, Y., and Wang, G.: Secondary
421 Formation of Atmospheric Brown Carbon in China Haze: Implication for an Enhancing Role of Ammonia, *Environ.*
422 *Sci. Technol.* 57, 11163-11172, <https://doi.org/10.1021/acs.est.3c03948>, 2023.
- 423 Lukács, H., Gelencsér, A., Hammer, S., Puxbaum, H., Pio, C., Legrand, M., Kasper-Giebl, A., Handler, M., Limbeck,
424 A., Simpson, D., and Preunkert, S.: Seasonal trends and possible sources of brown carbon based on 2-year aerosol
425 measurements at six sites in Europe, *J. Geophys. Res.* 112, <https://doi.org/10.1029/2006JD008151>, 2007.
- 426 Lopez-Hilfiker, F. D., Mohr, C., Ehn, M., Rubach, F., Kleist, E., Wildt, J., Mentel, T. F., Lutz, A., Hallquist, M.,
427 Worsnop, D., and Thornton, J. A.: A novel method for online analysis of gas and particle composition: description and
428 evaluation of a Filter Inlet for Gases and AEROSols (FIGAERO), *Atmos. Meas. Tech.* 7, 983-1001,
429 <https://doi.org/10.5194/amt-7-983-2014>, 2014.



- 430 Mohr, C., Lopez-Hilfiker, F. D., Zotter, P., Prevot, A. S. H., Xu, L., Ng, N. L., Herndon, S. C., Williams, L. R., Franklin,
431 J. P., Zahniser, M. S., Worsnop, D. R., Knighton, W. B., Aiken, A. C., Gorkowski, K. J., Dubey, M. K., Allan, J. D.,
432 and Thornton, J. A.: Contribution of Nitrated Phenols to Wood Burning Brown Carbon Light Absorption in Detling,
433 United Kingdom during Winter Time, *Environ. Sci. Technol.* 47, 6316-6324, <https://doi.org/10.1021/es400683v>, 2013.
- 434 Moise, T., Flores, J. M., and Rudich, Y.: Optical Properties of Secondary Organic Aerosols and Their Changes by
435 Chemical Processes, *Chem. Rev.* 115, 4400-4439, <https://doi.org/10.1021/cr5005259>, 2015.
- 436 Montoya-Aguilera, J., Horne, J. R., Hinks, M. L., Fleming, L. T., Perraud, V., Lin, P., Laskin, A., Laskin, J., Dabdub,
437 D., and Nizkorodov, S. A.: Secondary organic aerosol from atmospheric photooxidation of indole, *Atmos. Chem. Phys.*
438 17, 11605-11621, <https://doi.org/10.5194/acp-17-11605-2017>, 2017.
- 439 Moschos, V., Kumar, N. K., Daellenbach, K. R., Baltensperger, U., Prevot, A. S. H., and El Haddad, I.: Source
440 Apportionment of Brown Carbon Absorption by Coupling Ultraviolet-Visible Spectroscopy with Aerosol Mass
441 Spectrometry, *Environ. Sci. Tech. Let.* 5, 302+, <https://doi.org/10.1021/acs.estlett.8b00118>, 2018.
- 442 Moschos, V., Gysel-Beer, M., Modini, R. L., Corbin, J. C., Massabo, D., Costa, C., Danelli, S. G., Vlachou, A.,
443 Daellenbach, K. R., Szidat, S., Prati, P., Prevot, A. S. H., Baltensperger, U., and El Haddad, I.: Source-specific light
444 absorption by carbonaceous components in the complex aerosol matrix from yearly filter-based measurements, *Atmos.*
445 *Chem. Phys.* 21, 12809-12833, <https://doi.org/10.5194/acp-21-12809-2021>, 2021.
- 446 Palm, B. B., Peng, Q. Y., Fredrickson, C. D., Lee, B., Garofalo, L. A., Pothier, M. A., Kreidenweis, S. M., Farmer, D.
447 K., Pokhrel, R. P., Shen, Y. J., Murphy, S. M., Permar, W., Hu, L., Campos, T. L., Hall, S. R., Ullmann, K., Zhang,
448 X., Flocke, F., Fischer, E. V., and Thornton, J. A.: Quantification of organic aerosol and brown carbon evolution in
449 fresh wildfire plumes, *P. Natl. Acad. Sci. USA.* 117, 29469-29477, <https://doi.org/10.1073/pnas.2012218117>, 2020.
- 450 Park, R. J., Kim, M. J., Jeong, J. I., Youn, D., and Kim, S.: A contribution of brown carbon aerosol to the aerosol light
451 absorption and its radiative forcing in East Asia, *Atmos. Environ.* 44, 1414-1421,
452 <https://doi.org/10.1016/j.atmosenv.2010.01.042>, 2010.
- 453 Saarikoski, S., Niemi, J. V., Aurela, M., Pirjola, L., Kousa, A., Ronkko, T., and Timonen, H.: Sources of black carbon
454 at residential and traffic environments obtained by two source apportionment methods, *Atmos. Chem. Phys.* 21, 14851-
455 14869, <https://doi.org/10.5194/acp-21-14851-2021>, 2021.
- 456 Salvador, C. M. G., Tang, R. Z., Priestley, M., Li, L. J., Tsiligiannis, E., Le Breton, M., Zhu, W. F., Zeng, L. M., Wang,
457 H., Yu, Y., Hu, M., Guo, S., and Hallquist, M.: Ambient nitro-aromatic compounds - biomass burning versus secondary
458 formation in rural China, *Atmos. Chem. Phys.* 21, 1389-1406, <https://doi.org/10.5194/acp-21-1389-2021>, 2021.
- 459 Sandradewi, J., Prevot, A. S. H., Szidat, S., Perron, N., Alfarra, M. R., Lanz, V. A., Weingartner, E., and Baltensperger,
460 U.: Using aerosol light absorption measurements for the quantitative determination of wood burning and traffic
461 emission contributions to particulate matter, *Environ. Sci. Technol.* 42, 3316-3323, <https://doi.org/10.1021/es702253m>,
462 2008a.



- 463 Sandradewi, J., Prevot, A. S. H., Weingartner, E., Schmidhauser, R., Gysel, M., and Baltensperger, U.: A study of
464 wood burning and traffic aerosols in an Alpine valley using a multi-wavelength Aethalometer, *Atmos. Environ.* 42,
465 101-112, <https://doi.org/10.1016/j.atmosenv.2007.09.034>, 2008b.
- 466 Satish, R., Shamjad, P., Thamban, N., Tripathi, S., and Rastogi, N.: Temporal Characteristics of Brown Carbon over
467 the Central Indo-Gangetic Plain, *Environ. Sci. Technol.* 51, 6765-6772, <https://doi.org/10.1021/acs.est.7b00734>, 2017.
- 468 Shen, X. L., Vogel, H., Vogel, B., Huang, W., Mohr, C., Ramisetty, R., Leisner, T., Prévôt, A. S. H., and Saathoff, H.:
469 Composition and origin of PM_{2.5} aerosol particles in the upper Rhine valley in summer. *Atmos. Chem. Phys.* 19,
470 13189-13208. <https://doi.org/10.5194/acp-19-13189-2019>, 2019.
- 471 Siemens, K., Morales, A., He, Q., Li, C., Hettiyadura, A. P. S., Rudich, Y., and Laskin, A.: Molecular Analysis of
472 Secondary Brown Carbon Produced from the Photooxidation of Naphthalene, *Environ. Sci. Technol.*, 56, 3340-3353,
473 <https://doi.org/10.1021/acs.est.1c03135>, 2022.
- 474 Song, J. W., Saathoff, H., Gao, L. Y., Gebhardt, R., Jiang, F., Vallon, M., Bauer, J., Norra, S., and Leisner, T.:
475 Variations of PM_{2.5} sources in the context of meteorology and seasonality at an urban street canyon in Southwest
476 Germany, *Atmos. Environ.* 282, <https://doi.org/10.1016/j.atmosenv.2022.119147>, 2022.
- 477 Sumlin, B. J., Pandey, A., Walker, M. J., Pattison, R. S., Williams, B. J., and Chakrabarty, R. K.: Atmospheric
478 Photooxidation Diminishes Light Absorption by Primary Brown Carbon Aerosol from Biomass Burning, *Environ. Sci.*
479 *Technol. Lett.* 4, 540-545, <https://doi.org/10.1021/acs.estlett.7b00393>, 2017.
- 480 Teich, M., van Pinxteren, D., Kecorius, S., Wang, Z. B., and Herrmann, H.: First Quantification of Imidazoles in
481 Ambient Aerosol Particles: Potential Photosensitizers, Brown Carbon Constituents, and Hazardous Components,
482 *Environ. Sci. Technol.* 50, 1166-1173, <https://doi.org/10.1021/acs.est.5b05474>, 2016.
- 483 Teich, M., van Pinxteren, D., Wang, M., Kecorius, S., Wang, Z. B., Muller, T., Mocnik, G., and Herrmann, H.:
484 Contributions of nitrated aromatic compounds to the light absorption of water-soluble and particulate brown carbon in
485 different atmospheric environments in Germany and China, *Atmos. Chem. Phys.* 17, 1653-1672,
486 <https://doi.org/10.5194/acp-17-1653-2017>, 2017.
- 487 Thieringer, J. R. D., Szabadi, J., Meyer, J., and Dittler, A.: Impact of Residential Real-World Wood Stove Operation
488 on Air Quality concerning PM_{2.5} Immission, *Processes*, 10, 545, <https://doi.org/10.3390/pr10030545>, 2022.
- 489 Thompson, S. L., Yatavelli, R. L. N., Stark, H., Kimmel, J. R., Krechmer, J. E., Day, D. A., Hu, W., Isaacman-
490 VanWertz, G., Yee, L., Goldstein, A. H., Khan, M. A. H., Holzinger, R., Kreisberg, N., Lopez-Hilfiker, F. D., Mohr,
491 C., Thornton, J. A., Jayne, J. T., Canagaratna, M., Worsnop, D. R., and Jimenez, J. L.: Field intercomparison of the
492 gas/particle partitioning of oxygenated organics during the Southern Oxidant and Aerosol Study (SOAS) in 2013,
493 *Aerosol Sci. Technol.* 51, 30-56, <https://doi.org/10.1080/02786826.2016.1254719>, 2017.



494 Wang, Q., Ye, J., Wang, Y., Zhang, T., Ran, W., Wu, Y., Tian, J., Li, L., Zhou, Y., Hang Ho, S. S., Dang, B., Zhang,
495 Q., Zhang, R., Chen, Y., Zhu, C., and Cao, J.: Wintertime Optical Properties of Primary and Secondary Brown Carbon
496 at a Regional Site in the North China Plain, *Environ. Sci. Technol.* <https://doi.org/10.1021/acs.est.9b03406>, 2019a.

497 Wang, Q. Y., Han, Y. M., Ye, J. H., Liu, S. X., Pongpiachan, S., Zhang, N. N., Han, Y. M., Tian, J., Wu, C., Long, X.,
498 Zhang, Q., Zhang, W. Y., Zhao, Z. Z., and Cao, J. J.: High Contribution of Secondary Brown Carbon to Aerosol Light
499 Absorption in the Southeastern Margin of Tibetan Plateau, *Geophys. Res. Lett.* 46, 4962-4970,
500 <https://doi.org/10.1029/2019gl082731>, 2019b.

501 Wu, G., Wan, X., Gao, S., Fu, P., Yin, Y., Li, G., Zhang, G., Kang, S., Ram, K., and Cong, Z.: Humic-like substances
502 (HULIS) in aerosols of central Tibetan Plateau (Nam Co, 4730 m asl): Abundance, light absorption properties and
503 sources, *Environ. Sci. Technol.* 52, 7203–7211, <https://doi.org/10.1021/acs.est.8b01251>, 2018.

504 Xie, M., Chen, X., Hays, M. D., Lewandowski, M., Offenberg, J., Kleindienst, T. E., and Holder, A. L.: Light
505 Absorption of Secondary Organic Aerosol: Composition and Contribution of Nitroaromatic Compounds, *Environ. Sci.*
506 *Technol.* 51, 11607– 11616, <https://doi.org/10.1021/acs.est.7b03263>, 2017.

507 Yang, Z., Tsona, N. T., George, C., and Du, L.: Nitrogen-Containing Compounds Enhance Light Absorption of
508 Aromatic-Derived Brown Carbon, *Environ. Sci. Technol.* <https://doi.org/10.1021/acs.est.1c08794>, 2022.

509 Zeng, L. H., Zhang, A. X., Wang, Y. H., Wagner, N. L., Katich, J. M., Schwarz, J. P., Schill, G. P., Brock, C., Froyd,
510 K. D., Murphy, D. M., Williamson, C. J., Kupc, A., Scheuer, E., Dibb, J., and Weber, R. J.: Global Measurements of
511 Brown Carbon and Estimated Direct Radiative Effects, *Geophys. Res. Lett.* 47, <https://doi.org/10.1029/2020gl088747>,
512 2020.

513 Zhang, Y., Albinet, A., Petit, J.-E., Jacob, V., Chevrier, F., Gille, G., Pontet, S., Chrétien, E., Dominik-Sègue, M.,
514 Levigoureux, G., Močnik, G., Gros, V., Jaffrezo, J.-L., and Favez, O.: Substantial brown carbon emissions from
515 wintertime residential wood burning over France, *Sci. Total Environ.* 743, 140752,
516 <https://doi.org/10.1016/j.scitotenv.2020.140752>, 2020.

517

518

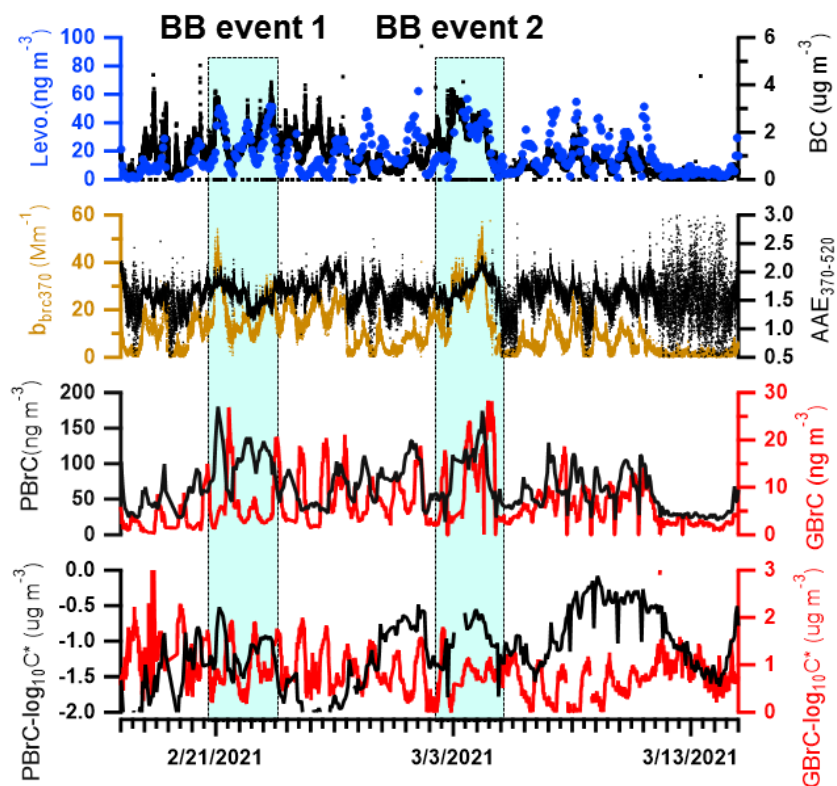
519

520

521

522

523

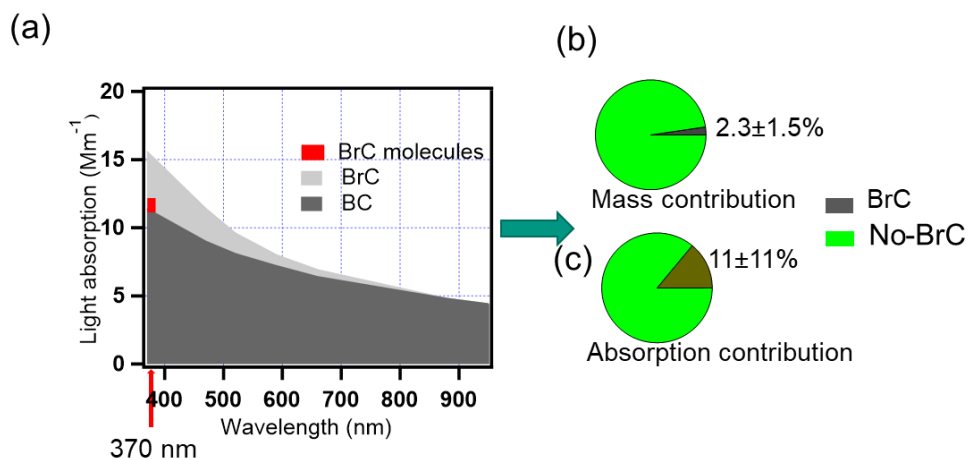


524

525 **Figure 1.** Time series of levoglucosan (Levo.) concentrations in particle phase from FIGAERO-CIMS, BC
 526 concentrations from aethalometer (AE33), absorption of brown carbon at 370 nm (b_{bc370}), absorption Ångström
 527 exponents between 370 nm and 520 nm ($AAE_{370-520}$), brown carbon concentrations in particle phase (PBrC) and
 528 gas phase (GBrC) and volatility ($\log_{10}C^*$) of brown carbon in particle phase (PBrC_ $\log_{10}C^*$) and gas phase
 529 (GBrC_ $\log_{10}C^*$) during the winter campaign.

530

531

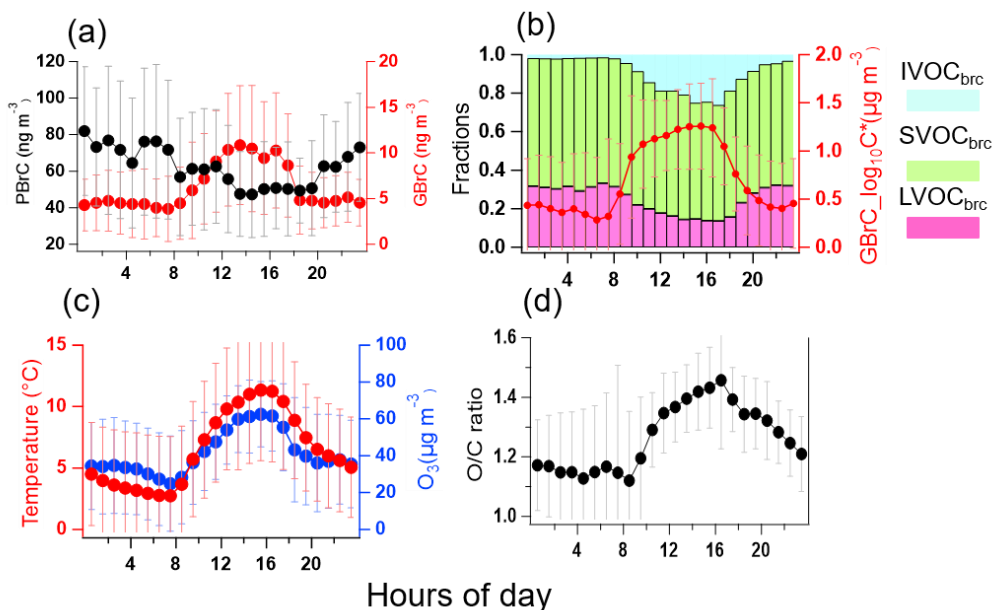


532

533 **Figure 2. (a) A stacked plot showing the main contributions to aerosol absorption from brown carbon and black**
534 **carbon based on the seven wavelengths measured by the aethalometer AE33. The contribution of the identified**
535 **brown carbon molecules to the total aerosol absorption is indicated in red at 370 nm. (b) Average mass**
536 **contribution of the potential BrC molecules to estimated total organic mass and (c) absorption contribution of**
537 **the potential BrC molecules identified to total absorption by BrC. The green pie: unidentified-BrC; the gray pie:**
538 **identified BrC.**

539

540

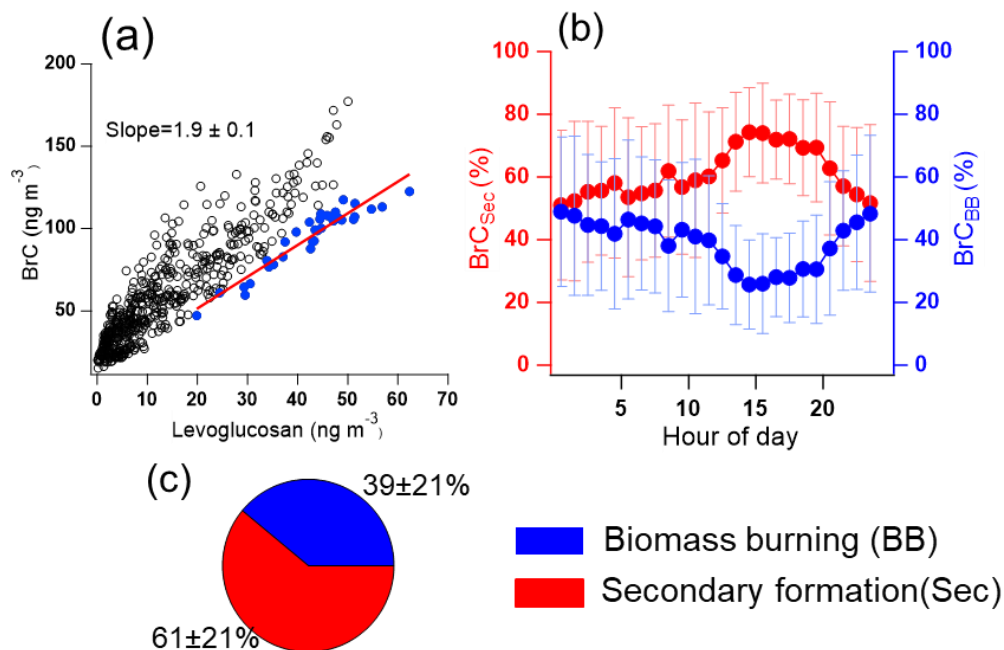


541

542 **Figure 3. Diurnal profiles averaged over the whole winter campaign of (a) BrC in the particle (PBrC) and gas**
 543 **phase (GBrC), (b) BrC volatility fractions in LVOC_{brC}, SVOC_{brC}, IVOC_{brC}, and mean BrC volatility in the gas**
 544 **phase (red line), (c) temperature and ozone concentration. (d) O/C ratio of the oxidized organic components in**
 545 **the gas phase.**

546

547



548

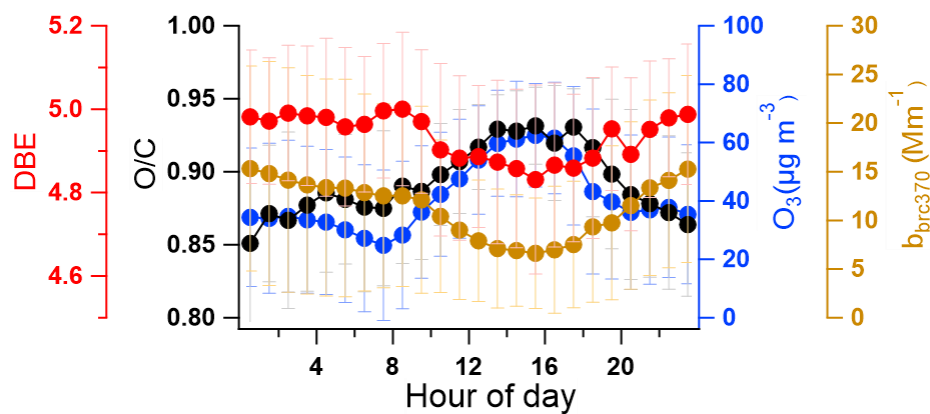
549 **Figure 4. (a) Correlation analysis of BrC and levoglucosan in the particle phase for the analysis of the**
550 **contribution of biomass burning using the edge method (Day et al., 2015). Blue points are the data used to**
551 **determine [BrC/lev.]_{BB}. (b) diurnal profile of secondary-formation BrC and biomass-burning BrC for the whole**
552 **measurement campaign. (c) Average mass fractions of secondary formed BrC and biomass-burning primary**
553 **BrC for the whole campaign.**

554

555



556



557

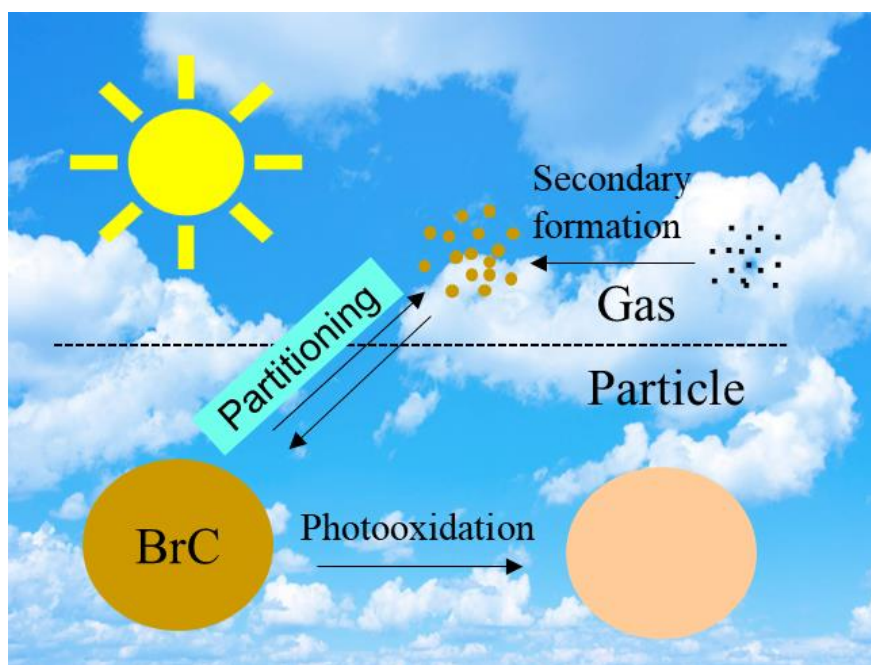
558 **Figure 5. The diurnal profile of DBE (double bond equivalent), O/C ratio of BrC, O₃, and b_{brC370} (absorption of**
559 **BrC at 370 nm) during the whole measured period.**

560

561



562



563

564 **Figure 6. A conceptual picture of the abstract**

565

566

567